

Chemical Science

Accepted Manuscript



This is an *Accepted Manuscript*, which has been through the Royal Society of Chemistry peer review process and has been accepted for publication.

Accepted Manuscripts are published online shortly after acceptance, before technical editing, formatting and proof reading. Using this free service, authors can make their results available to the community, in citable form, before we publish the edited article. We will replace this *Accepted Manuscript* with the edited and formatted *Advance Article* as soon as it is available.

You can find more information about *Accepted Manuscripts* in the [Information for Authors](#).

Please note that technical editing may introduce minor changes to the text and/or graphics, which may alter content. The journal's standard [Terms & Conditions](#) and the [Ethical guidelines](#) still apply. In no event shall the Royal Society of Chemistry be held responsible for any errors or omissions in this *Accepted Manuscript* or any consequences arising from the use of any information it contains.



www.rsc.org/chemicalscience

ARTICLE

Hierarchical Nanoscale Multi-shell Au/CeO₂ Hollow Spheres

Cite this: DOI: 10.1039/x0xx00000x

P. F. Xu^a, R. B. Yu^{*a}, H. Ren^a, L. B. Zong^a, J. Chen^a and X. R. Xing^aReceived 00th January 2012,
Accepted 00th January 2012

DOI: 10.1039/x0xx00000x

www.rsc.org/

Multi-shell ceria hollow spheres (MSCHSs) with uniform size of ~300nm and controlled shell number up to quadruple were synthesized by using carbonaceous spheres as the template in a combined process including the hydrothermally enhanced metal cation adsorption and tunable calcination. The featured sizes of these MSCHSs are hierarchical nanoscale, including the diameters of the interior and exterior hollow spheres (80~300nm), the thickness of the shells (~30nm), the distance between shells (<100nm), and the pore size in the shells (~4nm), which made the as-synthesized MSCHSs possess not only large specific surface area (~90 m² g⁻¹) and narrow mesopore distribution, but also nanosized interconnected chambers. With these structural characteristics, the MSCHSs show fascinating capacities as fine hosts for noble metals. Gold nanoparticles with sizes below 5nm could be loaded on these MSCHSs with high content and good dispersity to construct the effective catalysts, which demonstrated much improved catalytic performance for the reduction of *p*-nitrophenol. The optimal values of reaction rate constant (*k*) could reach up to 0.96 min⁻¹. Moreover, this approach opens up a new way to form nanosized multi-shell structures, especially those with large cations radii.

Introduction

Gold nanoparticles loaded on metal oxide supports with high surface area have demonstrated its high catalytic activity in many chemical process.¹⁻⁵ Besides the well accepted factors of the size, charge and dispersity of the gold nanoparticles, experimental and theoretical studies also revealed that the nature of the support, and the Au/support electronic interaction are crucial for determining the activity of the supported gold catalysts.⁶⁻⁹ Apparently, the selection of the support is important for constructing excellent catalyst. Ceria (CeO₂) was proved to be one of the ideal supports, combining with gold, other noble and transition metals, ceria shows high activity in many catalytic reactions mainly because of its possibility of reversible release and storage of lattice oxygen¹⁰ and the cooperativity between metal and ceria.¹¹⁻¹³ However, aggregations and structure collapse often occur under its work environment, which deteriorate the performance of ceria supported catalysts. So it is of great significance to design well-defined architectures to provide large surface area, numerous active sites, and generate separate nanoreactors against aggregation of Au nanoparticles and structure collapse of the catalyst.¹⁴⁻¹⁶

Among all kinds of well-defined architectures, hollow spheres, especially multi-shell hollow spheres have lots of

merits due to low density, large specific area, high permeability and confined interior space, which promote efficiency of loading and increase the contact surface between metal particles and supports. In comparison with the simple hollow sphere, the multi-shell one possesses more shells and isolated chambers. These constituent subunits often divide hollow interiors into several nanosized regions which reinforce size effects on material properties. Meanwhile, the two parameters could be finely regulated to optimize the design of heterogeneous catalysts. Endowing ceria with hollow architectures may make them not only expose more surface active sites and generate more separate nanoreactors against aggregation but also provide more free voids as buffer zones against structure collapse, so that a superior support for gold nanoparticles might be constructed.

So far, abundant strategies are designed to fabricate the unique hollow structures.¹⁷⁻¹⁹ Among these, hard template synthesis is a good choice because of its simple control, easy prediction for the targeted products and strong reproducibility.²⁰⁻²² Carbonaceous microspheres due to their rich surface hydrophilic functional groups (-OH and -COOH), good affinity with metal ions and accessible pore channels often serve as hard templates for hollow oxide spheres.²³ The formation of hollow structure consists mainly of the capture of metal cations and the removal of carbonaceous microspheres

through calcinations. Accurate control of the above two steps have allowed the fabrication of diverse hollow materials.^{20-21, 24} Though lots of transition metal oxide multi-shell structures have been produced, the synthesis of rare earth oxide multi-shell spheres rarely exists. The difficult synthesis is partly because that the radii of rare earth metal cations are much larger than those of transition metal cations. Moreover, the sizes of carbonaceous microspheres used in the literatures are usually large ($>1\mu\text{m}$), which result in a too long diffusion distance for large rare earth metal cations to move into the inner space of the carbonaceous spheres, and therefore obstructed hollow structure formation. Although in our previous research we have tried other way to synthesize multi-shell ceria, the low synthetic controllability is apparent.²⁵ In that work, the single-, double-, and triple-shell microspheres were obtained from three different synthetic systems. Additionally, the obtained hollow spheres with relatively large diameter of about $1\text{-}2\mu\text{m}$ and low specific surface area of $79.5\text{ m}^2\text{ g}^{-1}$ possessed pretty loose structure,²⁵ which might result in high possibility of structure collapse during their applications. Obviously, controlled synthesis of rare earth oxide multi-shell spheres is still a great challenge.

In the present work, small carbonaceous spheres with diameter of $\sim 600\text{nm}$ were chosen as template. Additionally, hydrothermal technique was employed to enhance the effective adsorption and diffusion of large cerium cations into carbonaceous spheres at the cation-adsorption stage. And the following controlled calcination with appropriate heat ramp rate would finally give a series of well crystallized MSCHSs. These spheres possess uniform size of $\sim 300\text{nm}$ in diameter and tunable shell numbers up to quadruple. This approach opens up a general way to the synthesis of multi-shell metal oxides hollow structures in the nanoscale, especially those with large metal cations. Moreover, gold nanoparticles with sizes below 5nm were effectively deposited and well dispersed on the synthesized MSCHSs. These Au/CeO₂ hollow spheres showed superior catalytic activity for the reduction of *p*-nitrophenol.

Results and discussion

The single-, double- and triple-shell ceria hollow nanospheres were harvested separately when the hydrothermally adsorbed carbonaceous spheres (ACSs) were calcined at heat ramp rate of 1°C min^{-1} , 2°C min^{-1} and $10^\circ\text{C min}^{-1}$ up to 500°C (holding time, 1h) (Fig.1a-c). The cross-linked spheres occurred at low heat ramp rate possibly due to higher cerium concentration on the external surface of carbonaceous spheres. The obtained MSCHSs possess uniform size of $\sim 300\text{nm}$, which is much smaller than reported multi-shell metal oxides spheres.^{20, 21, 24-28} Additionally, with hierarchical nanoscale featured sizes (e.g. the dimension of triple-shell sample (Fig. 1c and Fig. S1): the exterior, middle and interior shell is about 300nm , 180nm and 80nm respectively, and average shell thickness is 30nm , etc.), these MSCHSs might show peculiar size effects in potential applications. The XRD patterns of these ceria hollow spheres (Fig. S2) revealed that they are all belonged to the pure cubic

fluorite ceria (PDF No. 34-0394), and the heat ramp rate and time can also affect the crystallinity of the final product. And it was evident that the shell was composed of small primary particles and voids. HRTEM analysis and SAED pattern (Fig. 1e and f) also confirmed the ceria hollow spheres were cubic fluorite structure. Moreover, the morphology features of MSCHSs (Fig.1a-c) clearly indicated that the shell number increased with the heat ramp rate. When the heat ramp rates reached up to $15^\circ\text{C min}^{-1}$, some quadruple-shell structures also appeared (Fig. 1d). Besides, many other multi-shell metal oxide spheres with similar nanosizes were also successfully fabricated by use of this method (Fig. S3), which confirmed the generality of our approach.

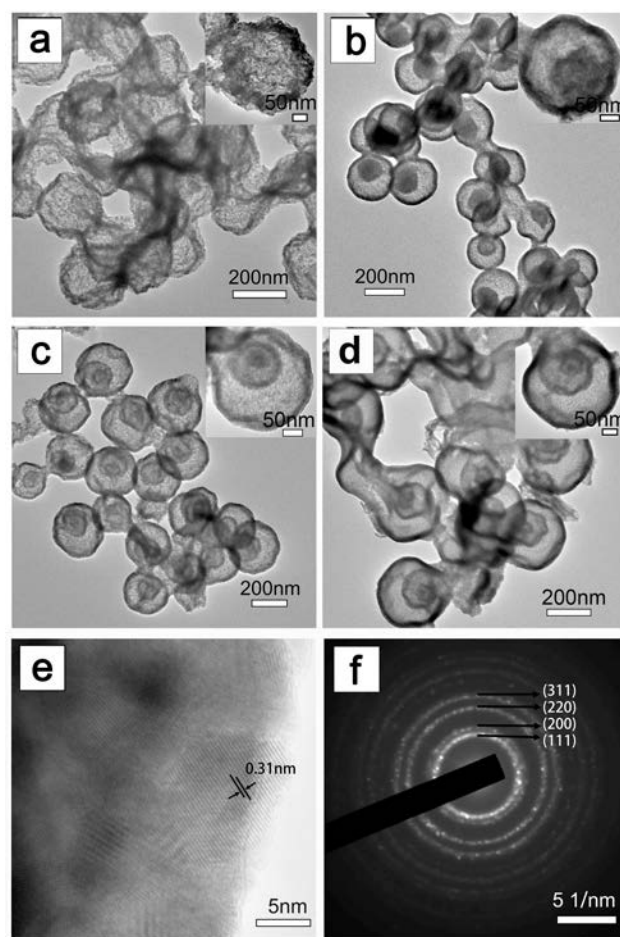


Fig. 1. (a-d) TEM images of ceria hollow nanospheres with various shell numbers obtained under the different heat ramp rate: (a) single shell, 1°C min^{-1} ; (b) double shell, 2°C min^{-1} ; (c) triple shell, $10^\circ\text{C min}^{-1}$; (d) quadruple shell, $10^\circ\text{C min}^{-1}$. Insets were the corresponding individual hollow sphere. (e-f) The characteristics of ceria hollow spheres with triple shell: (e) HRTEM image; (f) SAED pattern.

Hydrothermally enhanced adsorption of cerium cations is believed as the key process for MSCHSs formation. Under different hydrothermal temperature of 120°C , 160°C and 180°C and the same calcination condition, ceria with various

spherical morphologies were separately harvested (Fig. S4). Particularly, under hydrothermal condition of 180 °C and 3h the core-shell ceria powder could be directly obtained (Fig. S5). Apparently, hydrothermal condition can enhance not only the adsorption of cerium cations and the crystallization of ceria but also accelerate the oxidation of carbonaceous spheres. Additionally, with the increase of hydrothermal time, shell thickness increased due to higher adsorption capacity of cerium cations (Fig. S6), which made it easy to realize the tunable shell thickness. In comparison with reported method, hydrothermal adsorption provided stronger drive for cerium cations trap and reinforced the interaction between cerium cations and carbonaceous spheres, which finally led to high yields and multi-shell architectures.

The images of the immediate products clearly indicated the evolution of triple-shell ceria hollow spheres (Fig. S7), which went through core contraction and shell separation. It was known that both penetration depth of metal cations and temperature gradient along the radial direction of ACSs played an important role in the process.^{26, 29-31} The former was related to adsorbed environment (temperature, metal ions concentration, solvent polar and etc.) while the latter was determined by heat ramp rate of calcination. The fact that a series of hollow spheres with various shell numbers could be generated by calcining ACSs with the same penetration depth under heat ramp rate proved the occurrence of diffusion and redistribution of cerium species within ACSs during calcinations. Besides, the decomposition of organic species and crystallization of cerium precursor were also involved in the process (Fig. S8). TG-DTA curves showed the weight residue of the ACSs is ~15%, which is much higher than that of conventional adsorption (~4%)^{20, 26}, confirming enhanced adsorption effect of hydrothermal treatment for metal ions. Besides, it was also explicit that under hydrothermal treatment slight heterogeneous nucleation of ceria happened in the cerium precursors. This nucleation not only increased the yield of the final products but also affected subsequent calcination and crystallization behaviors.

On the basis of the evolution of MSCHSs discussed above, the illustration for the formation mechanism was deduced (Fig. 2). Firstly, carbonaceous spheres trapped cerium species through their surface functional groups and pore channels under mild hydrothermal condition to form ACSs, in which the adsorption, penetration and nucleation of cerium species might be dominant. Secondly, the redistribution of cerium species in ACSs happened during calcinations. As the heat ramp rate increased, the radius of temperature influence spread before the combustion of organic species, leading to deeper penetration of cerium species and final more shells. Thirdly, when the temperature reached the critical value, the combustion of organic species and crystallization of cerium species provided energy for the separation between cores and shells. Moreover, deeper penetration of cerium species led to more shells. Besides, core/shell structured ceria could be directly generated through higher temperature hydrothermal treatment.

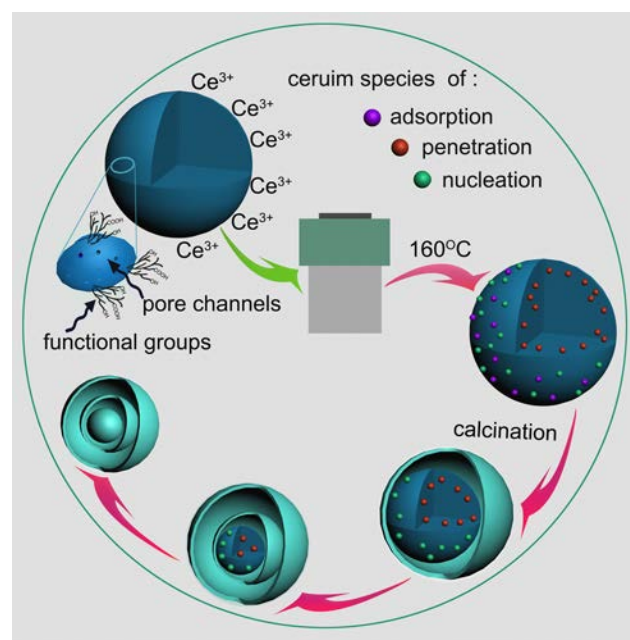


Fig. 2. Illustration for the formation mechanism of the triple-shell ceria hollow spheres.

The porous features in discrete shells were examined by means of nitrogen adsorption-desorption isotherm. The Brunauer-Emmett-Teller (BET) specific area of as-prepared MSCHSs are all around $90 \text{ m}^2 \text{ g}^{-1}$, which was higher than those of other reported multi-shell structures due to the smaller size.³² The specific area of the triple-shell ceria hollow spheres is $95.3 \text{ m}^2 \text{ g}^{-1}$ (Fig. S9). Its type IV adsorption-desorption isotherm curve with H4-type hysteresis loop indicated the presence of mesopore structure. The mesopore size distribution calculated by Barrett-Joyner-Halenda (BJH) model from the adsorption branch was narrow in the range of 1~5nm. In the Raman spectra of ceria hollow spheres with triple shell (Fig. S10), the weak band between 540cm^{-1} and 600cm^{-1} could prove the existence of oxygen vacancies.³³

With the high specific surface area and active sites, these MSCHSs might serve as promising supports for loading of noble metals to construct high performance catalyst. Here, gold nanoparticles was employed for the encapsulation of MSCHSs through the impregnation-reduction method.²⁸ Fig. 3a showed gold nanoparticles with diameters below 5nm were well dispersed over the entire shell of triple-shell ceria hollow spheres. Moreover, the embedded gold nanoparticles were strongly attached to the ceria supports, forming rich perimeter interfaces which may favor the catalytic reaction easily. The loading content of gold determined by ICP analysis was ca. 3.39wt%, much higher than 1.28wt% in the literature.²⁸ This high loading efficiency might arise from the larger specific area and more active sites of the MSCHSs. The lattice fringes of gold nanoparticles of 0.24nm is corresponding to the (111) planes of gold (Fig. 3b). The XPS detection (Fig. 3c) showed that the Au4f doublet peaks $4f_{7/2}$ and $4f_{5/2}$ appeared at 83.8ev and 87.5ev, respectively. Compared with the characteristic

value of bulk Au at 84.0 eV and 87.7 eV,^{34, 35} the negative shift (-0.2 eV) in binding energy occurred due to the electronic interaction between ceria supports and gold nanoparticles. As for the O 1s spectra, the peak at 531.6 eV appeared for ceria hollow spheres with gold nanoparticles loaded due to the interaction between gold nanoparticles and ceria host.

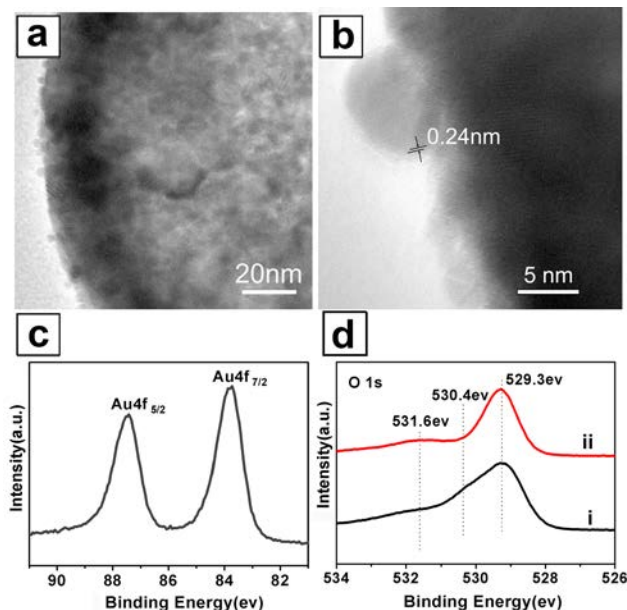


Fig. 3. (a) Representative TEM images; (b) HRTEM images; (c) Au 4f spectra of triple-shell ceria hollow spheres with Au nanoparticles supported; (d) O 1s spectra of triple-shell ceria hollow spheres (i) without and (ii) with Au nanoparticles supported.

The reduction of *p*-nitrophenol in the presence of NaBH₄ has been widely used as a model reaction to evaluate the catalytic ability of noble metals supported catalysts.³⁶⁻⁴⁰ The difference in absorption band of the reactant *p*-nitrophenol (centered at 400 nm) and the product *p*-aminophenol (centered at 300 nm) allowed the catalytic process to be monitored by UV-vis absorption spectra. The reaction cannot occur with the non-loaded MSCHSs (Fig. S11). When 50 μL catalyst (1.4 mg mL⁻¹) was injected into the reaction system as in the literature, the whole process was so quickly finished within 3 min that the data cannot be recorded in details. Hence, the amount of catalyst was decreased to 20 μL to monitor the process as shown in Fig. 4a. After the catalysts were added, the reduction reaction was triggered and the generated H₂ bubbles not only served as a reductant but also promoted mass transfer of reaction system. The characteristic absorption peaks of *p*-nitrophenol at 400 nm gradually disappeared within 18 min while the characteristic absorption peaks of *p*-aminophenol became stronger. Here the ratios of C_t and C₀, where are *p*-nitrophenol concentration at time *t* and 0 min, were determined by the relative absorption intensity at 400 nm, A_t/A₀. Since the amount of NaBH₄ largely exceeded that of *p*-nitrophenol, the catalytic reaction should follow first-order kinetics. And reaction rate constants *k* was

measured from the slope of plots of ln(C_t/C₀) vs time. The catalytic reaction over gold nanoparticles loaded MSCHSs and commercial CeO₂ were measured and corresponding results are shown in Fig. 4b, which revealed that the catalytic activity of the catalysts followed the order: triple shell > double shell > single shell >> commercial CeO₂. The nature of these

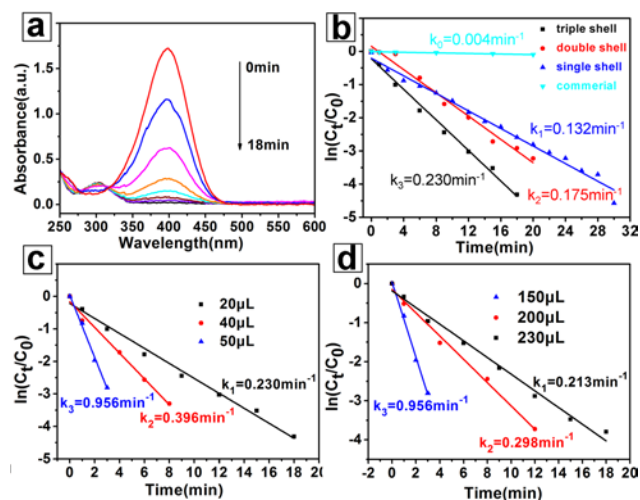


Fig. 4. (a) UV-vis spectra of the catalytic reduction of *p*-nitrophenol to *p*-aminophenol over Au/CeO₂ triple-shell spheres measured at different time intervals. (b) Plots of ln(C_t/C₀) vs time by use of Au loaded MSCHSs and commercial CeO₂ under the same test conditions. (c-d) Plots of ln(C_t/C₀) vs time over Au/CeO₂ triple-shell catalyst (c) with different catalyst amount, (d) with different *p*-nitrophenol amount.

hierarchical supports (such as large specific surface area, mesopores and small featured sizes) and the synergistic effects between gold nanoparticles and ceria supports which resulted in high loading content, good dispersion and optimized Au/CeO₂ electronic interaction are believed to be main reasons for their high activity. Moreover, the increase of catalytic activity with the shell number are also thought to be related to their confined interior space, which might provide more contact of reactant and catalyst, and then improve the reaction conversion.

On the basis of as-prepared catalysts with triple-shell structure, the influence of catalyst amount and *p*-nitrophenol amount on reaction rate constants *k* was explored in Fig. 4c-d. It was evident that the more addition of catalyst gave higher rate constants *k*, while increasing *p*-nitrophenol amount slowed down catalytic reaction. The active sites of catalyst occupied by reactants and diffusion-controlled mechanism in reaction solution might be the cause of the results.³⁶ In comparison of the catalytic activity of our hybrid catalysts with the reported values in terms of rate constant and turnover frequency (Table 1), the multi-shell Au/CeO₂ catalysts showed comparable turnover frequency and the highest rate constant. Additionally, after 8 cycles of catalytic reaction, the catalyst can keep its original morphology and activity (Fig. S12), indicating the excellent stability and long catalytic life. Obviously, the as-

synthesized MSCHSs with hierarchically nanoscaled featured size are the ideal support for gold nanoparticles, and these multi-shell Au/CeO₂ hybrids will certainly have promising potentials in the wider range of the exciting areas involved in gold catalysis.

Table 1. Catalytic activity comparison on the reduction of *p*-nitrophenol in the presence of noble metals loaded catalysts.

Noble metals loaded catalysts	T	k ^a	TOF ^b	Ref.
	(K)	(min ⁻¹)	(min ⁻¹)	
Au/CeO ₂ triple shell	298	0.96	4.60	Our work
Au-CeO ₂ yolk-shell	298	0.77	9.89	28
Pt@CeO ₂	297	0.43	1.50	36
Au@hm-ZrO ₂	298	0.31	---	37
Au-TiO ₂	298	0.79	---	38
Au@SiO ₂	298	0.84	---	39
RGO@Pd@C	298	---	4.56	40

^a First-order reaction rate constant. ^b Turnover frequency, which were estimated from the data given in corresponding references.

Experimental

Synthesis of carbonaceous spheres template: Carbonaceous spheres (CSs) were fabricated by hydrothermally according to the reference.²³ In the typical procedure, glucose (8g) with deionized water (80mL) was hydrothermally reacted at 180°C for 24h. And then the brown carbonaceous spheres powder with the average diameter of ~600nm (see Fig. S11) were collected by centrifugation, washed with distilled water and absolute alcohol in sequence, and finally dried in air at 80°C for 12 h.

Synthesis of multi-shell ceria hollow spheres (MSCHSs): carbonaceous spheres (50mg) were dispersed in deionized water (10mL) as solid templates, followed by adding Ce(NO₃)₃ solution (10mL, 0.5M). The mixture was adequately stirred for 45min and treated via ultrasonic vibration for another 45min, and then was hydrothermally treated at 160°C for 6h. After that, the dark brown ACSs powder was collected by centrifugation, washed with deionized water and absolute alcohol in sequence, and finally dried in air at 80°C for 12h. These ACSs went through calcinations under various heat ramp rates to generate a series of MSCHSs with different shell numbers. The single-, double-, triple- and quadruple-shell ceria hollow nanospheres were fabricated separately by heating the ACSs at heat ramp rate of 1°C min⁻¹, 2°C min⁻¹, 10°C min⁻¹ and 15°C min⁻¹ to 500°C (holding time, 1h) in air in Muffle furnace.

Synthesis of Au/CeO₂ hybrid nanostructures: As-prepared MSCHSs (28mg) were dispersed in deionized water (15mL) under magnetic stirring. Then, freshly prepared HAuCl₄ (500μL,

10mM) was added to the solution and agitated for 18h. Sequentially, the mixture was collected by centrifugation, washed with deionized water and redispersed in deionized water (30mL). After that, freshly prepared NaBH₄ (500μL, 30mM) was added to the redispersion. The purple powder was rinsed with deionized water until no chloride ions were probed by AgNO₃ test. Finally, Au/CeO₂ hybrid nanostructures were dried at 80°C for 12 h in vacuum.

Characterizations: X-ray diffraction (XRD) patterns were determined by a Philips XPert PRO MPD X-ray diffractometer operated at 35 kV with Cu-Kα radiation. Transmission electron microscopy (TEM), high-resolution transmission electron microscopy (HRTEM), selected area electron diffraction (SAED) and high-angle annular dark field (HAADF) STEM were carried out on a JEOL JEM-2100F transmission electron microscope with an accelerating voltage of 200 kV. Thermogravimetry-differential thermal analysis (TG-DTA) curves were recorded on a TG/DTA6300 thermoanalyzer at a linear heating rate of 10°C min⁻¹ under the atmosphere of air. The nitrogen adsorption-desorption isotherm curves were measured on a Quantachrome Instrument NOVA4000 at 77K. The loading content of gold determined by ICP-AES (IRIS, Intrepid II XSP, Thermo Electron, USA). The X-ray photoelectron spectra were conducted on a Kratos spectrometer (AXIS Ultra DLD, Shimadzu/Kratos, Ltd.) with monochromatic Al Kα radiation (hν =1486.6eV). The binding energies for all spectra were calibrated with respect to the C1s reference signal at 284.8eV. The Raman spectra were recorded on JY HR800 laser Raman spectrometer with 532nm excitation.

Catalytic reaction: *p*-nitrophenol (150μL, 1mM) and NaBH₄ solution (2mL, 100mM) were added into a quartz cuvette. The aqueous solution containing Au/CeO₂ hybrid nanostructures (20μL, 1.4mg mL⁻¹) was injected into the cuvette to trigger the reaction and the catalytic process was recorded by UV-vis spectroscopy as a function of time.

Conclusions

In summary, by using smaller carbonaceous spheres as the hard template, ceria hollow nanospheres with multiple shells and mesopores were fabricated with high yields. Hydrothermal treatment that enhanced the adsorption and penetration of cerium cations into carbonaceous spheres is believed to be the key process for the formation of these MSCHSs. These MSCHSs with large specific surface area, narrow mesopore distribution and nanosized interconnected chambers can sever as a superior supports for gold nanoparticles to build well-performed hybrid catalysts. The as-synthesised multi-shell Au/CeO₂ hollow spheres showed high activity and long life in catalytic reduction of *p*-nitrophenol. Moreover, this strategy could be extended to synthesize other multi-shell metal oxides especially those with large metal cations. Additionally, the featured sizes of these multi-shell architectures are all below visible light wavelength, which are also attractive for photonics and electronics. Much effort is being devoted to probing the

exact formation mechanism and potential applications for these complex hollow structures.

Acknowledgements

This work was financially supported by the National Natural Science Foundation of China (No. 51072020, 21271021, 21031005). Special thanks to prof. Dan Wang (Institute of Process Engineering, Chinese Academy of Sciences, China) for his valuable discussion and worthwhile advice.

Notes and references

^a Department of Physical Chemistry, School of Metallurgical and Ecological Engineering, University of Science and Technology Beijing, 100083, China. ranboyu@ustb.edu.cn

Electronic Supplementary Information (ESI) available: XRD patterns; Raman spectra; Nitrogen adsorption-desorption isotherm curves; Representative TEM images. See DOI: 10.1039/b000000x/

- I. X. Green, W. J. Tang, M. Neurock and J. T. Jr, *Science*, 2011, **333**, 736-739.
- M. Haruta, *Nature*, 2005, **437**, 1098-1099.
- A. Corma and P. Serna, *Science*, 2006, **313**, 332-334.
- A. A. Herzog, C. J. Kiely, A. F. Carley, P. Landon and G. J. Hutchings, *Science*, 2008, **321**, 1331-1335.
- Z. F. Bian, T. Tachikawa, P. Zhang, M. Fujitsuka and T. Majima, *J. Am. Chem. Soc.*, 2014, **136**, 458-465.
- M. Valden, X. Lai and D. W. Goodman, *Science*, 1998, **281**, 1647-1650.
- R. J. Davis, *Science*, 2003, **301**, 926-927.
- N. Acerbi, S. C. Edman Tsang, G. Jones, S. Golunski and P. Collier, *Angew. Chem. Int. Ed.*, 2013, **52**, 7737-7741.
- M. Cargnello, V. V. T. Doan-Nguyen, T. R. Gordon, R. E. Diaz, E. A. Stach, R. J. Gorte, P. Fornasiero and C. B. Murray, *Science*, 2013, **341**, 771-773.
- A. Trovarelli, *Catal. Rev. Sci. Eng.*, 1996, **38**, 439-520.
- Q. Fu, H. Saltsburg and M. Flytzani-Stephanopoulos, *Science*, 2003, **301**, 935-938.
- J. A. Farmer and C. T. Campbell, *Science*, 2003, **329**, 933-936.
- A. Tanaka, K. Hashimoto and H. Kominami, *J. Am. Chem. Soc.*, 2012, **134**, 14526-14533.
- R. Si and M. Flytzani-Stephanopoulos, *Angew. Chem. Int. Ed.*, 2008, **47**, 2884-2887.
- Z. Jin, M. D. Xiao, Z. H. Bao, P. Wang and J. F. Wang, *Angew. Chem. Int. Ed.*, 2012, **51**, 6404-6410.
- K. Yoon, Y. Yang, P. Lu, D. H. Wan, H. C. Peng, K. S. Masias, P. T. Fanson, C. T. Campbell and Y. N. Xia, *Angew. Chem. Int. Ed.*, 2013, **51**, 9543-9546.
- Y. D. Yin, R. M. Rioux, C. K. Erdonmez, S. Hughes, G. A. Somorjai and A. P. Alivisatos, *Science*, 2004, **304**, 711-714.
- J. Li and H. C. Zeng, *J. Am. Chem. Soc.*, 2007, **129**, 15839-15847.
- M. H. Oh, T. Yu, S. H. Yu, B. Lim, K. T. Ko, M. G. Willinger, D. H. Seo, B. H. Kim, M. G. Cho, J. H. Park, K. Kang, Y. E. Sung, N. Pinna and T. Hyeon, *Science*, 2013, **340**, 964-968.
- X. Y. Lai, J. Li, B. A. Korgel, Z. H. Dong, Z. M. Li, F. B. Su, J. Du, and D. Wang, *Angew. Chem. Int. Ed.*, 2011, **50**, 2738-2741.
- J. Y. Wang, N. L. Yang, H. J. Tang, Z. H. Dong, Q. Jin, M. Yang, D. Kisailus, H. J. Zhao, Z. Y. Tang and D. Wang, *Angew. Chem. Int. Ed.*, 2013, **52**, 6417-6420.
- A. Primo, T. Marino, A. Corma, R. Molinari and H. Garcia, *J. Am. Chem. Soc.*, 2011, **133**, 6960-6963.
- X. M. Sun and Y. D. Li, *Angew. Chem. Int. Ed.*, 2004, **43**, 597-601.
- Z. H. Dong, X. Y. Lai, J. E. Halpert, N. L. Yang, L. X. Yi, J. Zhai, D. Wang, Z. Y. Tang and L. Jiang, *Adv. Mater.*, 2012, **24**, 1046-1049.
- J. Qi, K. Zhao, G. D. Li, Y. Gao, H. J. Zhao, R. B. Yu and Z. Y. Tang, *Nanoscale*, 2014, **6**, 4072-4077.
- Y. Zeng, X. Wang, H. Wang, Y. Dong, Y. Ma and J. N. Yao, *Chem. Commun.*, 2010, **46**, 4312-4314.
- L. J. Han, R. J. Liu, C. S. Li, H. H. Li, G. J. Zhang and J. N. Yao, *J. Mater. Chem.*, 2012, **22**, 17079-17085.
- C. M. Fan, L. F. Zhang, S. S. Wang, D. H. Wang, L. Q. Lu and A. W. Xu, *Nanoscale*, 2012, **4**, 6835-6840.
- J. G. Guan, F. Z. Mou, Z. G. Sun and W. D. Shi, *Chem. Commun.*, 2010, **46**, 6605-6607.
- L. Zhou, D. Y. Zhao and X. W. Lou, *Adv. Mater.*, 2012, **24**, 745-748.
- L. Zhou, H. Y. Xu, H. W. Zhang, J. Yang, S. B. Hartono, K. Qian, J. Zou and C. Z. Yu, *Chem. Commun.*, 2013, **49**, 8695-8697.
- X. Y. Lai, J. Li, B. A. Korgel, Z. H. Dong, Z. M. Li, F. B. Su, J. Du and D. Wang, *Angew. Chem. Int. Ed.*, 2011, **50**, 2738-2741.
- M. Guo, J. Q. Lu, Y. N. Wu, Y. J. Wang and M. F. Luo, *Langmuir*, 2011, **27**, 3872-3877.
- M. Turner, V. B. Golovko, O. Vaughan, P. Abdulkin, A. B. Murcia, M. S. Tikhov, B. F. G. Johnson and R. M. Lambert, *Nature*, 2008, **454**, 981-983.
- J. Li, C. Y. Liu and Y. Liu, *J. Mater. Chem.*, 2012, **22**, 8426-8430.
- X. Wang, D. P. Liu, S. Y. Song and H. J. Zhang, *J. Am. Chem. Soc.*, 2013, **135**, 15864-15872.
- X. Q. Huang, C. Y. Guo, J. Q. Zuo, N. F. Zheng and G. D. Stucky, *Small*, 2009, **5**, 361-365.
- Y. H. Deng, Y. Cai, Z. K. Sun, J. Liu, C. Liu, J. Wei, W. Li, C. Liu, Y. Wang and D. Y. Zhao, *J. Am. Chem. Soc.*, 2010, **132**, 8466-8473.
- J. Lee, J. C. Park and H. Song, *Adv. Mater.*, 2008, **20**, 1523-1528.
- Z. Y. Zhang, F. Xiao, J. B. Xi, T. Sun, S. Xiao, H. R. Wang, S. Wang and Y. Q. Liu, *Sci. Rep.*, 2014, **4**, 4053.